Laser-Induced Fluorescence Studies of Excited Sr Reactions.[†] 1. Sr(^{3}P$_1$) + HF

J. M. Teule,[‡] J. Mes, J. Bulthuis,* M. H. M. Janssen,* and S. Stolte*,§

*Lasercentre and Department of Chemistry, Vrije Universiteit, De Boelelaan 1083,
1081 HV Amsterdam, The Netherlands*

Received: April 24, 1998; In Final Form: July 6, 1998

Electronic ground-state SrF (X$^2\Sigma$) products formed in the reaction of electronically excited Sr(^{3}P$_1$) with HF are studied using laser-induced fluorescence (LIF) detection. Sr atoms are excited to the ^{3}P$_1$ state using a frequency-narrowed and -stabilized linear titanium−sapphire laser at 689.3 nm. The vibrational and rotational population distributions in the SrF(X$^2\Sigma$) products are deduced from the LIF spectra of the B$^2\Sigma$−X$^2\Sigma$ and A$^2\Pi_{3/2}$−X$^2\Sigma$ transitions using spectrum simulation. The results show a strong dependence of the SrF internal energy distribution on the impact parameter. The light H atom is ejected with high translational energy.

1. Introduction

Chemical reactions of electronically excited atoms involve higher potential energy surfaces with other symmetry and topological properties than the ground-state potential, influencing the reactivity, branching ratios, and rovibronic population distribution in the product molecule.[1,2] It is generally observed that the total energy of a reactive system is not the key parameter determining the reaction mechanism, cross sections, and product energy distributions.[3] Laser-induced fluorescence (LIF) studies, in which the product state distributions are directly determined under single-collision conditions, can supply detailed information necessary for elucidation of the reaction mechanism.

This study concentrates on the reaction

$$\text{Sr}(^3\text{P}_1) + \text{HF}(v=0) \rightarrow \text{SrF}(\text{X}^2\Sigma, v', J') + \text{H}$$
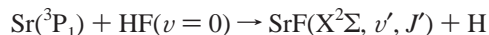
Over the past 20 years, gas-phase reactions between alkaline earth metals (Ca, Sr, Ba) and HF have been frequently studied (e.g., refs 4−10). These reactions are especially interesting since they involve a transformation from a covalently bound reagent to an ionically bound product. Previous studies concern the reactions at various collision energies, with both ground-state and internally excited reactants. For the reactions with the alkaline earth metal in the electronic ground state, generally a competition between a direct reaction (where the metal abstracts the F-atom from the molecule) and an insertion mechanism is assumed.[4] Which mechanism is dominant is determined by the specific details of the potential energy surface on which the reaction evolves.

The energetics of the Sr + HF reaction, which is endoergic when both reactants are in the ground state, is shown in Figure 1. Several studies have been performed on this reaction with the HF molecule either vibrationally or rotationally excited, or varying the collision energy.[4−7,10] They show that the product vibrational distribution is essentially the same when the reaction energy is supplied as reagent vibration or translation.[5,6] In the reactions Sr + HF(v = 1) and Sr + HF(v = 2) 21%[4,7] and 22%[6] of the available energy is released as vibrational energy

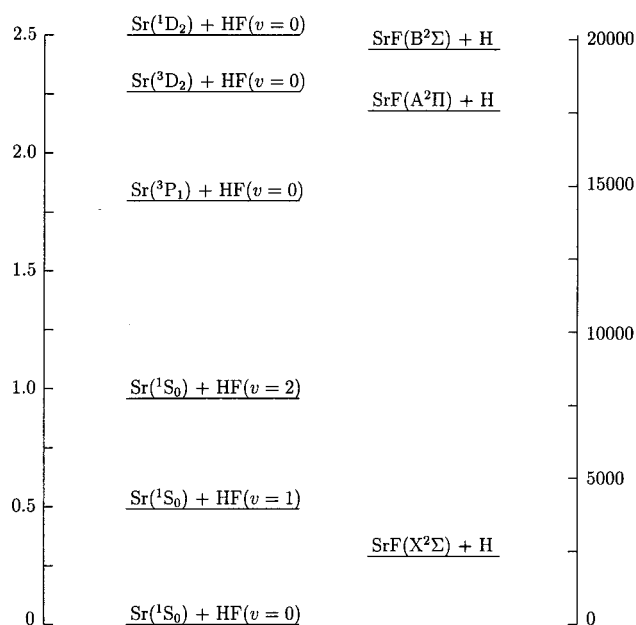**Figure 1.** Energetics for the Sr + HF reaction system (energy left axis in eV, right axis in cm^{-1}). The spin−orbit splittings in the Sr(^{3}P$_J$) state are 186.8 cm^{-1} between $J = 0$ and $J = 1$, and 394.2 cm^{-1} between $J = 1$ and $J = 2$.[20]

of the product, respectively. Zhang et al.[4] demonstrated the sensitivity of the product vibrational distribution to the rotational energy of the reagent; in the reaction with rotationally excited HF, higher vibrational levels were populated than when the same amount of energy was supplied as vibrational energy. They explained this by assuming a direct (abstraction) reaction, apparently being promoted by reagent rotation, resulting in a nonstatistical vibrational population distribution.

Loesch and Stienkemeier studied the effect of reagent alignment on the total reaction cross section.[10] The experimental results suggest a bent transition state on the reaction path, as has also been predicted for the Ca + HF reaction.[11]

The Sr + HF reaction is often considered as a H + H′L → HH′ + L (H, H′ = heavy, L = light) reaction. The conservation of total angular momentum demands that $\mathbf{J}_{\text{reag}} + \mathbf{L}_{\text{reag}} = \mathbf{J}_{\text{prod}} + \mathbf{L}_{\text{prod}}$, where $\mathbf{J}$ is the rotational angular momentum and $\mathbf{L}$ is

LIF Studies of Excited Sr Reactions

J. Phys. Chem. A, Vol. 102, No. 47, 1998 **9483**

the orbital angular momentum ($|\mathbf{L}| = \mu b v$, μ = reduced mass, b = impact parameter, v = relative velocity). For H + H'L → HH' + L reactions, generally $\mathbf{J}_{reag} \approx 0$, $\mathbf{L}_{prod} \approx 0$, so $|\mathbf{J}_{prod}| \approx |\mathbf{L}_{reag}| = \mu b v_i$, where v_i is the initial relative velocity of the reagents.[12] This constraint, in principle, allows the determination of the impact parameter distribution for reactive collisions into a specific vibrational level, v (opacity function), from the product rotational distribution, since a certain (b, v_{reag}) pair leads to one specific (v, J) product state. For our system the kinematic restriction is relaxed as we will discuss later. In the reaction of Sr with HF, a large amount of energy is released as product translation. Despite the considerable number of experimental studies, the detailed dynamical features of this reaction are not understood.

There have been several studies of chemical reactions involving electronically excited Sr and Ca, where generally the influence of the form of reagent energy on the reaction cross section and product electronic state branching ratios is studied.[2,13-16] Reactions through the electronic excitation of the van der Waals precursor Ca-HX have also been investigated.[17] In most cases the (relative) reaction cross sections strongly depend on the initial spin-orbit state of the excited metal atom.[2] It is believed that the distinct alignment of the atomic orbitals results in different energy surfaces owing to electrostatic interactions. From the different surfaces the charge transfer occurs with differing probabilities, influencing the reactive cross sections. In a study of Han et al.[18] the effect of the electronic excitation on the internal state distributions of the ground-state products was determined for the reactions of $Ca(^1S_0, {}^3P_1)$ with CH_2Cl_2 and $CHCl_3$. Although the population of higher vibrational states increases when the Ca atom is electronically excited, the fraction of the available energy disposed into vibration decreases. The increase in fractional rotational energy suggests that most of the electronic energy is transferred into the rotation of the product molecule.

In their study of the reaction $Ca(^3P_J, {}^1D)$ + HF, Engelke and Meiwes-Broer[16] determined the internal energy distributions in $CaF(X^2\Sigma)$ using laser-induced fluorescence detection. They estimated a specific opacity function $P_{v=0}$ (b) for this system, neglecting the velocity dependence of the reaction cross section. The rotational distribution suggests contributions from only a limited range of impact parameters in the formation of CaF(X, $v = 0$) products. No specific opacity functions for higher product vibrational states have been deduced.

For the reaction $Sr(^3P_1)$ + HF($v = 0$), the chemiluminescent channels are closed (see Figure 1). In 1978 Solarz et al.[8] studied this reaction, using pulsed laser excitation to produce metastable Sr and detecting the $SrF(X^2\Sigma)$ product by laser-induced fluorescence (LIF). Only a rough estimate of the amount of energy released into vibration (~40%) was presented. They explained the difference with the reaction of ground-state Sr, stating that the ionic state mixes in at larger intermolecular distances on the excited state surface compared to the ground-state surface, resulting in an early energy release and consequently more product vibration.

The present study uses a beam-gas setup, in which a beam of Sr atoms is excited using a frequency-stabilized continuous wave titanium-sapphire laser.[19] The ground-state SrF molecules are detected using LIF, which allows accurate determination of both vibrational and rotational population distributions in the product. Spectrum simulation is applied to extract the available information from the measured spectra. In the last section the experimental observations are discussed and interpreted.
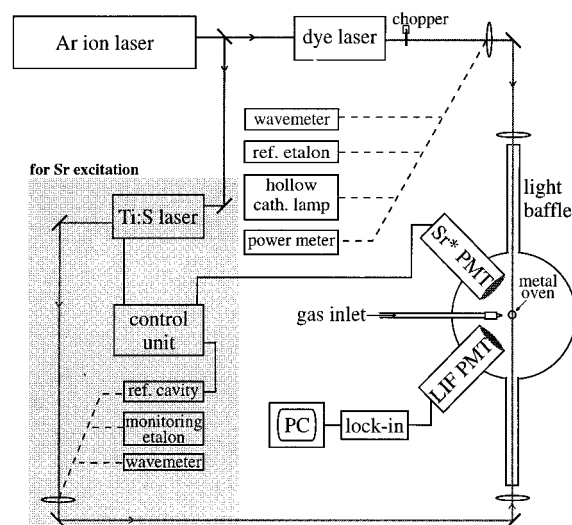

Figure 2. Experimental setup. The LIF detection setup is the same as in previous experiments.[21] For constant Sr excitation a control unit locks a reference cavity on the $Sr(^3P_1)$ fluorescence signal. The laser frequency is locked on the reference cavity.

2. Experimental Section

Figure 2 shows the experimental setup, consisting of a vacuum system[21] and two laser systems. The high-vacuum chamber contains an effusive metal oven, in which the Sr metal is heated to about 900 K. The vapor pressure of about 0.1 Torr inside the oven results in a number density of Sr atoms in the reaction zone of about 3×10^{10} cm^{-3}.[22] The ground-state Sr atoms are excited to the metastable $(5s5p(^3P_1))$ state (radiative lifetime 19.6 μs[23]) using a frequency-stabilized linear Ti:sapphire laser.

An argon ion laser (Spectra Physics model 2030, 15 W output all lines) pumps the modified Ti:sapphire laser (Spectra Physics model 3900S, 600-1000 nm), which contains a birefringent filter, a thin Etalon (FSR 200 GHz), and a temperature-stabilized thick Etalon (FSR 20 GHz). With 4 W pump power the Ti: sapphire laser output is typically 300 mW at 689.3 nm in two laser modes, separated by 200 MHz. One of the longitudinal modes (effective bandwidth ~ 6 MHz) is used to excite the Sr atoms. Part of the laser output is used to lock the laser on an external reference cavity (750 MHz), which is locked on the $Sr(^3P_1)$ fluorescence signal to keep the number density of excited atoms constant. The laser power in the scattering chamber is approximately 70 mW. The laser is slightly focused by a lens with a focal length $f = 1$ m. Using this setup we estimate that about 2% of the Sr atoms in the reaction zone is electronically excited.

The molecular reactant HF is kept at constant pressure in an ice-cooled stainless steel vessel. The vapor is led into the reaction chamber through a needle valve to give a typical pressure of 7×10^{-5} Torr (number density 2×10^{12} cm^{-3}). Cold traps (liquid nitrogen) are incorporated into the vacuum tube system to prevent contamination and deterioration of the system by the highly corrosive HF gas.

To allow LIF detection, the SrF ground-state reaction products are excited to either the $B^2\Sigma$ state (577-587 nm) or the $A^2\Pi_{3/2}$ state (644-653 nm), using a modified tunable linear dye laser (Spectra Physics model 375, bandwidth 10 GHz) pumped with 3.5 W from the Ar$^+$ laser mentioned above. In the detection zone the dye laser power is approximately 35 mW. The dye laser beam is modulated by a mechanical chopper at a frequency

TABLE 1: Spectroscopic Constants (in cm^{-1}) for the X$^2\Sigma$, A$^2\Pi$, and B$^2\Sigma$ Electronic States of SrF, Used in the Simulations

	Dunham coefficients	X$^2\Sigma$	A$^2\Pi$	B$^2\Sigma$
T_e	Y_{00}		15221.094[a,b]	17267.42[c]
ω_e	Y_{10}	502.4[c]	510.5[d]	495.8[c]
$\omega_e x_e$	$-Y_{20}$	2.27[c]	2.34[a,e]	2.34[c]
B_e	Y_{01}	0.25053[f]	0.25374[a,b]	0.249409[a,f]
$\alpha_e \times 10^3$	$-Y_{11} \times 10^3$	1.546[f]	1.56[d]	1.565[a,f]
$\gamma_e \times 10^6$	$Y_{21} \times 10^6$	2.23[f]	1.5[a]	1.4[f]
$D_e \times 10^7$	$Y_{02} \times 10^7$	2.4987[f]	2.3[a,b]	2.52[f]
γ_D	γ_{00}	0.0025[f]		0.13498[f]
$\alpha_\gamma \times 10^4$	$-\gamma_{10} \times 10^4$	0.164[f]		4.95[f]
A_e			264.34[a,d]	
$\alpha_A \times 10^3$			-0.5[a]	
$A_{D_e} \times 10^5$			-9.4[g]	
p_e			-0.133[g]	
$q_e \times 10^4$			-1.1[g]	

[a] Adjusted to fit the experimental spectra. [b] Reference 29. [c] Reference 26. [d] Reference 30. [e] Reference 4. [f] Reference 27. [g] Reference 28.

TABLE 2: Franck−Condon Factors for the $\Delta v = 0$ Sequences of the A$^2\Pi$−X$^2\Sigma$ and B$^2\Sigma$−X$^2\Sigma$ Transitions in SrF, Used in the Simulations

v	A$^2\Pi$	B$^2\Sigma$	v	A$^2\Pi$	B$^2\Sigma$
0	0.9834	0.9974	11	0.6662	0.9048
1	0.9509	0.9919	12	0.6411	0.8922
2	0.9192	0.9859	13	0.6165	0.8789
3	0.8883	0.9794	14	0.5923	0.8648
4	0.8582	0.9724	15	0.5686	0.8499
5	0.8288	0.9684	16	0.5451	0.8342
6	0.8001	0.9566	17	0.5219	0.8176
7	0.7721	0.9477	18	0.4990	0.8002
8	0.7447	0.9381	19	0.4764	0.7819
9	0.7180	0.9277	20	0.4541	0.7627
10	0.6918	0.9167			

TABLE 3: Calculated Bandhead Positions (in cm^{-1}), Using the Spectroscopic Constants in Table 1, in the $\Delta v = 0$ Sequence of the B$^2\Sigma$−X$^2\Sigma$ and A$^2\Pi_{3/2}$−X$^2\Sigma$ Transitions in SrF, and Rotational Levels at Which They Are Formed[a]

	B$^2\Sigma$				A$^2\Pi_{3/2}$			
	R_1		R_2		P_2		Q_2/P_{21}	
v	ν	N''	ν	N''	ν	N''	ν	N''
0	17 298.6	148	17 321.6	183	15 313.5	107	15 351.6	42
5	17 258.8	135	17 280.2	170	15 354.4	104	15 390.3	40
10	17 215.5	120	17 235.1	154	15 390.5	104	15 425.3	41
15	17 169.0	105	17 186.7	138	15 421.8	107	15 456.7	42
20	17 119.5	90	17 135.2	121	15 448.2	113	15 484.2	47

[a] N is the rotational quantum number, where $N = J - S$, with J the total angular momentum (quantum number J) and S the electron spin (quantum number $S = 1/2$).

of 120 Hz. The wavelength is calibrated using an etalon, a hollow cathode lamp, and a wavemeter (Burleigh).

The fluorescence emitted by the SrF products is both spatially and color-filtered to suppress the Sr($^3P_1$) fluorescence light. The light is projected onto the red sensitive cathode of a photomultiplier tube (RCA C31034). In the saturated LIF spectra polarization effects can be ignored. The signal is phase-sensitively amplified and recorded as a function of excitation wavelength using a PC. The LIF spectrum of the A$^2\Pi_{3/2}$−X$^2\Sigma$ is recorded using a narrow-band interference filter (Melles Griot, $\lambda = 650$ nm, fwhm = 10 nm) to suppress the Sr($^3P_1$) fluorescence more effectively.

3. Spectrum Simulation

The internal state distribution of SrF was derived from the LIF spectra using the same simulation procedure as described previously.[21] In a CW-LIF experiment where saturation is achieved, the fluorescence signal is directly related to the flux of the product molecules. This is in contrast to pulsed LIF, where the signal is proportional to the density of molecules.[24,25] Therefore, the population distributions as derived from the spectra directly reflect the relative state-specific reaction cross sections.

The rovibronic line positions are calculated using the available spectroscopic data. The B$^2\Sigma$ state was studied by Steimle et al.[26] and Ernst and Schröder,[27] and their spectroscopic constants were sufficient to reproduce our spectra. Slight adjustment of the B_e and α_e parameters was necessary because of the high rotational levels populated. The A$^2\Pi$ state was only studied for low vibrational states, but using the constants presented in refs 28−30 and improving the v-dependent parameters we are able to simulate the A$^2\Pi_{3/2}$ spectrum. The product population distributions, deduced from the LIF spectra, do not critically depend on a perfect match of the line positions. Therefore, we have aimed at a good overall agreement between the experimental and simulated spectra, instead of trying to determine the spectroscopic constants with high accuracy. The spectroscopic constants used in the simulations are presented in Table 1. The $\Delta v = 0$ sequences of the A$^2\Pi$ and B$^2\Sigma$ states are measured, since they are the strongest transitions. The Franck−Condon factors for these transitions are obtained from refs 30 and 31, respectively (Table 2). For the A$^2\Pi$ state the values for $v = 16$−20 had to be extrapolated.

Owing to the similarity of the excited- and ground-state vibrational and rotational constants, the Fortrat parabolas (transition frequencies as a function of the rotational quantum number) can reach an extremum. This results in the formation of bandheads in the R$_1$ and R$_2$ branches of the B$^2\Sigma$ state and the P$_2$ and P$_{21}$/Q$_2$ branches of the A$^2\Pi_{3/2}$ state. The rotational constant B'_v in the B$^2\Sigma$ state is slightly smaller than B''_v in the ground state, which means that the R$_1$, R$_2$ branches form bands shaded to the red. B'_v (A$^2\Pi$), on the other hand, is larger than B''_v, resulting in P$_2$, P$_{21}$/Q$_2$ bandheads shaded to the blue. Similarly, the differences between the vibrational constants of the ground and excited states cause the bandheads to shift to the red for increasing v in the B$^2\Sigma$−X$^2\Sigma$ spectrum, whereas they shift to the blue for increasing v in the A$^2\Pi_{3/2}$−X$^2\Sigma$ spectrum. The rotational quantum numbers at which the different bandheads are formed are presented in Table 3 for several vibrational levels. Since the bandheads for a single vibrational level are formed at different rotational levels and are clearly separated in the spectrum, their intensity ratio is critically dependent on the rotational population distribution. The latter can therefore be determined accurately, although single rotational lines are not resolved in the experimental spectrum. The margins of error in the peak position of $P_v(N)$ are estimated to range from better than ±2% for the lowest v values to ±5% for the highest v values. The accuracy of the width of $P_v(N)$ is estimated to be within about ±10%.

For the calculation of the reaction energy, the internal energy distribution function of the HF molecule at 300 K, E_{int}, is convoluted with the collision energy distribution function E_{col}. The resulting distribution function is then shifted upward by the reaction exothermicity ($D_0^\circ(SrF) - D_0^\circ(H-F) + E_{Sr(^3P_1)}$) to give the available energy $\langle E_{avl}\rangle$. The energy values are presented in Table 4.

The intensity of each line was weighted by an assumed vibrational population $P(v)$ and a v-dependent rotational popula-

LIF Studies of Excited Sr Reactions

J. Phys. Chem. A, Vol. 102, No. 47, 1998 **9485**

TABLE 4: Reaction Energetics (in eV)

	Sr + HF
$\langle E_{int} \rangle$	0.039
$\langle E_{col} \rangle$	0.072
D_0^o(HF)	5.881 ± 0.001^a
D_0^o(SrF)	5.59 ± 0.07^a
$E_{Sr(^3P_1)}$	1.798^b
$\langle E_{avl} \rangle$	1.62 ± 0.07
spread $(E_{avl})^c$	0.12

[a] Reference 32. [b] Reference 20. [c] The spread is the width of the distribution function E_{avl} (fwhm).
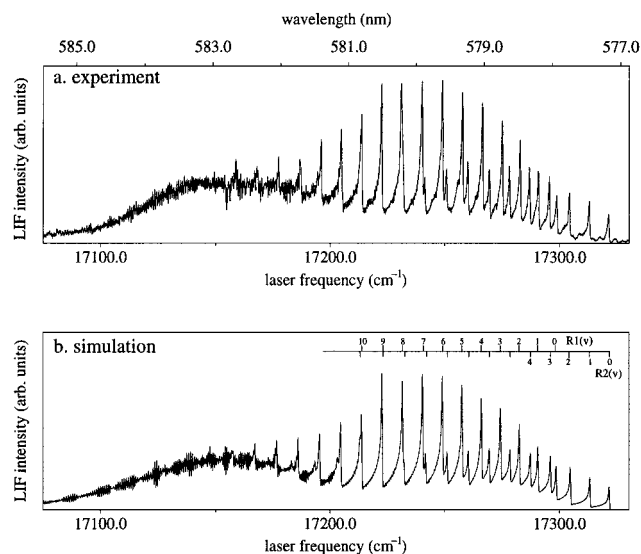
Figure 3. Experimental (a) and simulated (b) spectra of SrF formed in the reaction of Sr($^3P_1$) with HF. The $B^2\Sigma - X^2\Sigma$, $\Delta v = 0$ sequence is shown. For the simulation the spectroscopic constants of Table 1 are used, as well as the vibrational and rotational state distributions shown in Figure 5. A Gaussian frequency profile with a fwhm of 0.4 cm^{-1} is used for the convolution. In the simulated spectrum the R_1 (marks pointing upward) and R_2 bandheads are indicated. The wiggle-like structure at the red side, which is also found in the calculated spectrum, is due to partially resolved rotational lines in the tails of the R-bands.

tion $P_v(N)$. The LIF spectrum was calculated assuming a Gaussian frequency profile, corresponding to the frequency profile of the excitation laser. The parameters specifying the vibrational and rotational distributions are varied until the experimental spectrum is reproduced.

4. Results

Figures 3a and 4a present the experimental LIF spectra of SrF formed in the reaction Sr($^3P_1$) + HF → SrF($X^2\Sigma$, v', J') + H. Shown are the $B^2\Sigma - X^2\Sigma$ transition and the $A^2\Pi_{3/2} - X^2\Sigma$ transition, respectively. The simulation results for both sequences are presented in Figures 3b and 4b. The input vibrational and rotational population distributions used in both simulations are also depicted (Figure 5).

The $A^2\Pi_{3/2} - X^2\Sigma$ spectrum shows that a contribution of SrF formed in the oven has to be taken into account. Some of the HF molecules diffuse into the Sr oven where high-temperature reactions take place. Product molecules are subsequently carried to the reaction region undergoing numerous thermalizing collisions. Though the number density of thermal product molecules is small, their contribution to the LIF spectrum is visible in the $A^2\Pi_{3/2} - X^2\Sigma$ spectrum around 15 352 cm^{-1}. The Q_2/P_{21} branch in this band forms bandheads at low J's, resulting
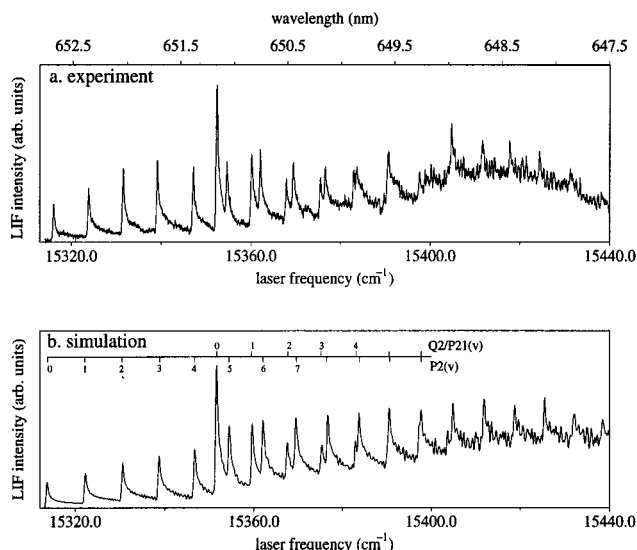

Figure 4. Experimental (a) and simulated (b) spectra of SrF formed in the reaction of Sr($^3P_1$) with HF. The $A^2\Pi_{3/2} - X^2\Sigma$, $\Delta v = 0$ sequence is shown. For the simulation the same spectroscopic constants and population distributions as in Figure 3 are used. A 4% contribution of SrF formed in oven reactions was taken into account. A Gaussian frequency profile with a fwhm of 0.4 cm^{-1} is used for the convolution. In the simulated spectrum the Q_2/P_{21} (marks pointing upward) and P_2 bandheads are indicated.

in high-intensity bands for $v = 0$, 1 in the thermal spectrum, as is illustrated in Figure 6.

A superposition of a spectrum calculated using the populations shown in Figure 5 and a thermal spectrum at 900 K in a ratio of 25:1 is sufficient to obtain the simulation result (Figure 4b). The 4% contribution of the thermal SrF products is hardly visible in the $B^2\Sigma - X^2\Sigma$ spectrum, since no bandheads are formed at the relatively low J's populated, and the background level between 17 250 and 17 300 cm^{-1} rises only slightly.

Because of the narrow-band interference filter used in the LIF detection of the $A^2\Pi_{3/2} - X^2\Sigma$ band, only the $\Delta v = 0$ fluorescence is measured, whereas in the $B^2\Sigma - X^2\Sigma$ measurements also off-diagonal fluorescence is collected. Consequently, the detection efficiency in the former experiment decreases for increasing vibrational excitation. This is accounted for in the simulation, multiplying the calculated LIF intensity by the Franck–Condon factors for the $\Delta v = 0$ transitions.

In the simulations a correction for saturation by optical pumping is made, multiplying the intensity of each rovibronic line by an optical pumping factor $1/(1 - 0.8q_{v'v''})$, as was introduced by Keijzer et al.[24] Here $q_{v'v''}$ is the Franck–Condon factor of the $v' \leftrightarrow v''$ transition. Although our experiments are inconclusive about the exact value of the correction factor (taken as 0.8), it is clear that saturation due to optical pumping occurs. The power dependence of the LIF signal is nonlinear, and it was not possible to satisfactorily simulate the spectra for both electronic transitions with the same population distributions when no saturation was included. Accounting for the various loss processes using this v-dependent optical pumping factor yields a good agreement between the experimental and simulated spectra for both transitions, using the same vibrational and rotational population distributions. Additional line broadening due to saturation[22] is taken into account by using a laser frequency profile with fwhm = 0.4 cm^{-1}.

The rotational distributions used in the simulations are Gaussian distributions, with N_{peak} decreasing from $N = 135$ for $v = 0$ to $N = 85$ for $v = 15$. From the simulations the average product vibrational, rotational, and translational energies are
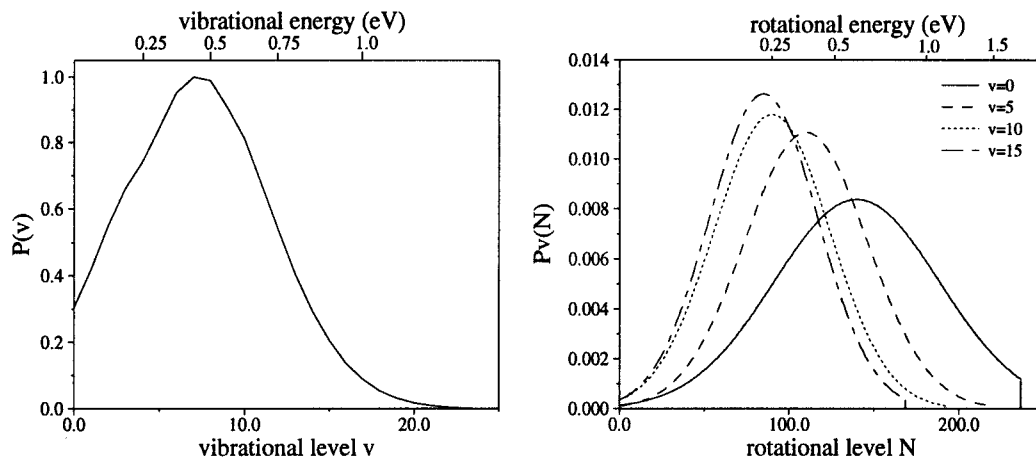
Figure 5. Input vibrational and rotational population distributions used in the simulated LIF spectrum of SrF formed in the reaction $Sr(^3P_1) + HF$. The vibrational distribution is a slightly adjusted Gaussian distribution in energy peaked at 0.40 eV and with a width of 0.61 eV (fwhm). The rotational state distributions are Gaussian distributions in N, peaked at $N = 140$ for $v = 0$ decreasing to $N = 85$ for $v = 15$. Since $\langle E_{avl} \rangle$ is used as a cutoff energy in the simulations, the rotational distribution for $v = 0$ is cut off at $N = 237$.
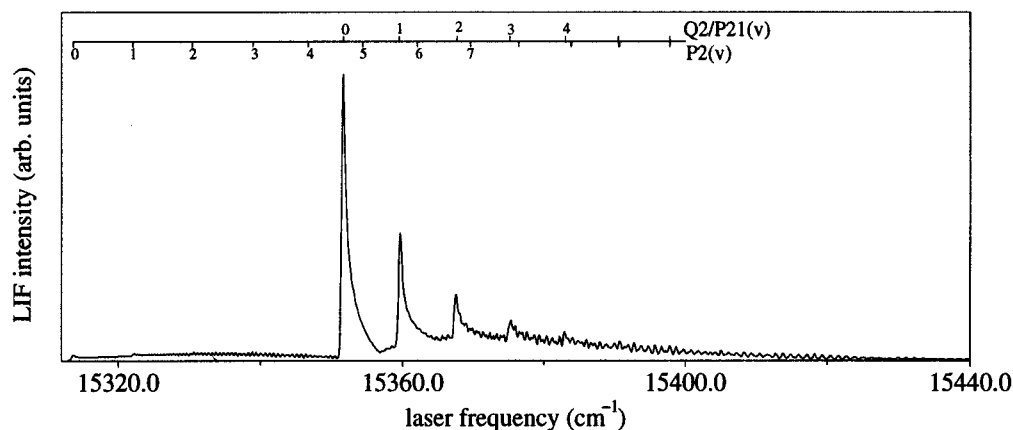
Figure 6. Simulated spectrum of SrF formed in the oven reaction of Sr with HF. The $A^2\Pi_{3/2}-X^2\Sigma$, $\Delta v = 0$ sequence is shown. The SrF vibrational and rotational state distributions are thermal with temperatures $T_v = T_r = 900$ K. The bandheads are indicated as in Figure 4.

TABLE 5: Average Product Energies of SrF Formed in the Reaction of $Sr(^3P_1)$ and HF

	SrF(X$^2\Sigma$)		
$\langle E_v \rangle$	0.45 eV	$\langle f_v \rangle$	0.28
$\langle E_r \rangle$	0.36 eV	$\langle f_r \rangle$	0.22
$\langle E_t \rangle$	0.81 eV	$\langle f_t \rangle$	0.50

determined; see Table 5. The fractional energies are calculated from $\langle f_E \rangle = \langle E \rangle / \langle E_{avl} \rangle$.

5. Discussion

This study qualitatively confirms earlier findings that product energy distributions, and therefore the reaction mechanism, are not predominantly determined by the total energy of the reaction. Although electronic excitation of the Sr atoms results in an excess energy of 1.62 eV, still only 28% is disposed into vibrational energy, compared to 21% found in earlier studies[4,6] for the reaction $Sr(^1S_0) + HF(v = 1, 2)$. These values are lower than the 40% product vibrational energy given by Solarz et al.,[8] but these authors gave only a rough estimate. Apparently, the use of electronic energy to surmount the endothermic reaction barrier does not significantly change the relative product energy disposal, compared to reactions with other forms of reagent energy (vibration,[5,6] translation[9]).

Figure 7 presents a triangle plot showing the experimentally determined energy distribution over vibration, rotation, and
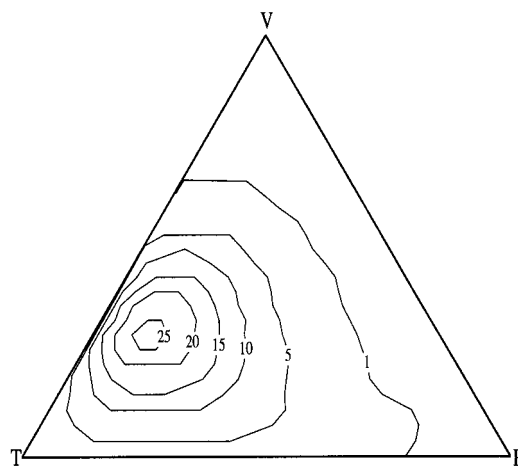

Figure 7. Triangular (semiclassical) plot of energy disposal in the $Sr(^3P_1) + HF(v = 0)$ reaction. The experimental results are displayed as contours of relative populations in a triangular coordinate system (see text). The vertexes represent the situation where all energy is released into one degree of freedom.

translation in the SrF products formed in the $Sr(^3P_1) + HF(v = 0)$ reaction. The vertexes represent the extreme situations, where all energy is disposed into one degree of freedom.[3] Permitted combinations of energy fractions f_v, f_r, and f_t with a certain probability give contours of equal probability $P(f_v, f_r, f_t)$. The

LIF Studies of Excited Sr Reactions

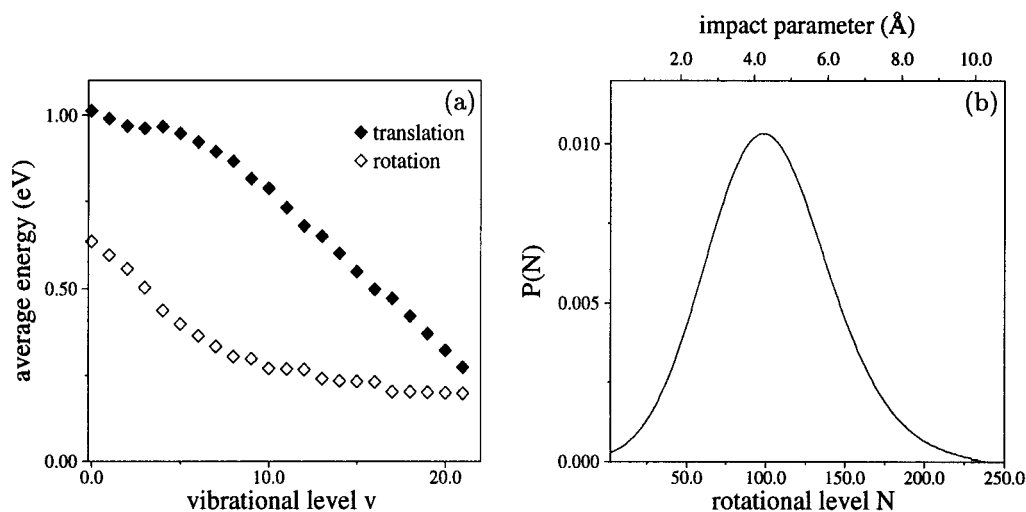*J. Phys. Chem. A, Vol. 102, No. 47, 1998* **9487**

Figure 8. (a) Average translational and rotational energy in the products as a function of vibrational quantum number. (b) Product rotational distribution $P(N) = \sum_v P(v) \, P_v(N)$, with $\sum_N P(N) = 1$. The upper axis gives the impact parameter as can be calculated assuming the kinematic constraint to be valid, i.e., $|\mathbf{J}_{prod}| \approx |\mathbf{L}_{reag}| = \mu b v_i$, where $J_{prod} = N$ if the $S = {}^1/_2$ contribution is neglected.

most probable (f_v, f_r, f_t) lies in the center of the contour plot, with a steep hill toward the $f_r = 0$ line. The $P(f_v, f_r, f_t)$ surface descends more slowly in the direction of the lower right $f_v = f_t = 0$ vertex, owing to the increasing rotation for lower vibrational levels.

The bell-shaped vibrational energy distribution (Figure 5) suggests that the reaction is dominated by a direct (abstraction) mechanism, which often results in a nonstatistical population distribution.[4]

In Figure 8a the average translational and rotational energy in the reaction products is displayed as a function of the vibrational quantum number. For low v, until $v = v_{peak} = 7$, the average rotational energy decreases linearly, and with a steeper slope than for $v > 7$. A similar correlation between vibration and rotation was also observed by Tsekouras et al.[36] for the reaction Ba + HI, a prototypical example of a kinematically constrained reaction. They observed that the maximum in the rotational distribution shifted from $J = 420$ for $v = 0$ to $J = 106$ for $v = 18$.

Noda and Zare[37] developed a model for kinematically constrained reactions, by assuming the relative recoil energy in the products to be constant, independent of the impact parameter b and the initial relative velocity v_i. They suggest that these reactions under some circumstances evolve through a critical configuration from which the light atom is ejected with constant translational energy for any impact parameter and collision energy. Some general features predicted by this "constant product recoil" (CPR) model are observed in our experiment, although in our case $\mathbf{L}_{prod}$ is not negligible, and the average product translational energy is only constant for low v's (see Figure 8). The model predicts a bell-shaped product vibrational distribution, peaked at a vibrational energy equal to the reaction energy minus the product recoil energy. It also implies that small impact parameters produce highly vibrationally excited products with consequently low rotational excitation, whereas large impact parameters cause products to be highly rotationally excited with low vibrational energy. Furthermore, the average rotational energy associated with each vibrational level is predicted to decrease linearly with increasing v up to $v = v_{peak}$, followed by a more slowly changing behavior.

The experimental observations from this work show remarkable agreement with the predictions of the CPR model. A bell-shaped product vibrational distribution is determined, in contrast with the distributions found for $Sr(^1S_0) + HF(v = 1, 2)$.[6] Highly vibrationally excited products show low rotational excitation and vice versa. The average rotational energy as a function of vibration decreases linearly up to $v = 7$, whereafter the slope decreases, as can be seen in Figure 8. The peak of the product vibrational distribution as calculated from the CPR model would be at $v = 11$, somewhat higher than the observed $v_{peak} = 7$.

About 50% of the available energy in the $Sr(^3P_1) + HF$ reaction is transferred into relative translation of the product. Although the reduced mass of the products (1.0 amu) is considerably lower than the reduced mass of the reagents (16.3 amu), the high amount of translational energy in the product (0.81 eV) makes the orbital angular momentum of the products of the same order of magnitude as $|\mathbf{L}_{reag}|$. $|\mathbf{L}_{prod}| = \mu_{SrF-H} v_f b_f$ can be estimated, using the average translational energy $\langle E_{col} \rangle$ and taking an upper limit estimate for b_f from $R_e(HF) + {}^1/_2 R_e(SrF) = 1.96$ Å ($R_e(HF) = 0.92$ Å, $R_e(SrF) = 2.075$ Å),[33] which gives $|\mathbf{L}_{prod}| \approx 38.7$ $\hbar$. With $|\mathbf{J}_{prod}|$ from the average rotational energy, $\mathbf{L}_{prod}$ cannot be completely neglected, and the kinematic constraint, as presented in section 1, should therefore rather be described as $\mathbf{J}_{prod} + \mathbf{L}_{prod} \approx \mathbf{L}_{reag}$. However, according to calculations by Hijazi and Polanyi,[40] $\mathbf{L}_{prod}$ has a slightly higher probability to be oriented antiparallel with respect to $\mathbf{J}_{prod}$ for $H + H'L \rightarrow HH' + L$ reactions. We are unable to account for the different possible orientations of $\mathbf{L}$ with respect to $\mathbf{J}$, which determine the actual contribution of $\mathbf{L}_{prod}$. Alternatively, we could make the simplification that $\mathbf{L}_{prod}$ is spherically distributed, in accordance with the constant product orbital alignment (CPOAM) model proposed by Hartree et al.[41] This model is a modification of the CPR model, the modification being the additional assumption of a constant-product orbital angular momentum L_{prod}, with a spherical distribution of $\mathbf{L}_{prod}$. Hartree et al. applied their model to the reaction $Xe(^3P_2) + HBr \rightarrow XeBr(B) + H$ by fitting $Z_m = L_{prod}/L_{reag}$ to measured values of the product rotational alignment for different collision energies. In our experiment we obtain directly from the LIF spectra the energy distribution over E_r and, from energy conservation, E_t for each vibrational product level v, without varying the collision energy. Furthermore, we have not done alignment experiments on the product rotational state distribution, so we are unable to estimate the orbital angular momentum ratio Z_m.

Owing to our lack of information on the collision energy dependence of the various quantities, we will therefore only consider the consequences of neglecting the contribution of $\mathbf{L}_{\text{prod}}$ as a limiting case. Then the kinematic constraint $|\mathbf{J}_{\text{prod}}| \approx |\mathbf{L}_{\text{reag}}| = \mu b v_i$ can be used to get an impression of the product yield as a function of the impact parameter. In this case v_i is chosen to be the average initial relative velocity. Figure 8b presents the product rotational distribution summed over v, $P(N)$, as a function of the rotational quantum number (lower axis), and as a function of the impact parameter of the reactants (upper axis). This distribution peaks at $b = 4.2$ Å, and impact parameters up to $b = 9$ Å are suggested to contribute to the reaction. The impact parameter corresponding to $\langle E_{\text{r}} \rangle = 0.36$ eV is 4.6 Å, corresponding to a reaction cross section $\sigma_{\text{r}} \approx 70$ Å^2. This estimate assumes a reaction probability of unity for the given impact parameter, i.e., assuming absence of any mechanism, such as steric hindrance, that would reduce the reaction probability for this impact parameter.

This estimated value is of the same order of magnitude as the values presented by Engelke and Meiwes-Broer[16,38] for the reaction Ca(^3P_J) + HF. Using similar calculations, they found the reaction cross section to be 100 Å$^2 \leq \sigma_{\text{r}} \leq 170$ Å^2. For this reaction, with $\langle E_{\text{avl}} \rangle = 1.54$ eV, they found that 25% of the reaction energy is disposed into product vibration, and 27% into rotation, which is also similar to our observations. These σ_{r} values, estimated by Engelke and Meiwes-Broer and in this study, are much larger than the $\sigma_{\text{r,max}} = 7.1$ Å^2 presented by Wüstenbecker[42] for the SrF($v = 0$) product from the reaction with ground-state Sr at a high collision energy (0.6 eV). It is clear that electronic excitation of the atomic reactant causes a large increase in the reaction cross section.

The probability distribution in Figure 8b peaks at 4.2 Å, which is close to the estimated harpooning radius (From R_h (Å) = 14.4/(IP − EA), with IP = ionization potential Sr($^3P_1$) = 3.9 eV and EA = electron affinity HF = 0.355 eV (theoretical prediction from ref 39)) of 4.1 Å. The electron jump mechanism is often believed to be a suitable representation of the mechanism for the M + RX, X$_2$ reactions (M = alkali metal, alkaline earth metal; X = halogen).[3,21,43] In this picture an electron jumps from the metal atom to the molecular reactant, resulting in a strong Coulombic force pulling the reactants together. The low ionization potential of Sr($^3P_1$) facilitates an electron jump. This mechanism could cause the observed inverted product vibrational distribution.

Summarizing, we have demonstrated that the product energy distribution in SrF formed in the Sr($^3P_1$) + HF reaction strongly depends on the impact parameter. Large impact parameters contribute to the reaction, resulting in high rotational excitation for low vibrationally excited products. The nonstatistical vibrational population distribution suggests that a direct reaction mechanism is more important for this reaction than the insertion mechanism. The light H-atom is ejected with high translational energy, taking up about 50% of the available energy.

References and Notes

(1) Gonzales-Urena, A.; Vetter, R. *J. Chem. Soc., Faraday Trans.* **1995**, *91*, 389; *Int. Rev. Phys. Chem.* **1996**, *15*, 377.

(2) Dagdigian, P. J.; Campbell, M. L. *Chem. Rev.* **1987**, *87*, 1.

(3) Levine, R. D.; Bernstein, R. B. *Molecular reaction dynamics and chemical reactivity*; Oxford University Press: New York, 1987.

(4) Zhang, R.; Rakestraw, D. J.; McKendrick, K. G.; Zare, R. N. *J. Chem. Phys.* **1988**, *89*, 6283.

(5) (a) Karny, Z.; Estler, R. C.; Zare, R. N. *J. Chem. Phys.* **1978**, *69*, 5199. (b) Karny, Z.; Zare, R. N. *J. Chem. Phys.* **1978**, *68*, 3360. (c) Man, C.; Estler, R. C. *J. Chem. Phys.* **1981**, *75*, 2779.

(6) Torres-Filho, A.; Pruett, J. G. *J. Chem. Phys.* **1982**, *77*, 740.

(7) Altkorn, R.; Bartoszek, F. E.; Dehaven, J.; Hancock, G.; Perry, D. S.; Zare, R. N. *Chem. Phys. Lett.* **1983**, *98*, 212.

(8) Solarz, R. W.; Johnson, S. A.; Preston, R. K. *Chem. Phys. Lett.* **1978**, *57*, 514.

(9) Gupta, A.; Perry, D. S.; Zare, R. N. *J. Chem. Phys.* **1980**, *72*, 6237.

(10) (a) Loesch, H. J.; Stienkemeier, F. *J. Chem. Phys.* **1994**, *100*, 740. (b) Loesch, H. J.; Stienkemeier, F. *J. Chem. Phys.* **1994**, *100*, 4308.

(11) Jaffe, R. L.; Pattengill, M. D.; Mascarello, F. G.; Zare, R. N. *J. Chem. Phys.* **1987**, *86*, 6150.

(12) Herschbach, D. R. *Adv. Chem. Phys.* **1966**, *10*, 319.

(13) Garay, M.; Esteban, M. E.; Verdasco, E.; González Ureña, A. *Chem. Phys.* **1995**, *195*, 235.

(14) Kierzkowski, P.; Pranszke, B.; Kowalski, A. *Chem. Phys. Lett.* **1996**, *254*, 391.

(15) Ding, G.; Sun, W.; Yang, W.; Xu, D.; Zhao, R.; He, G.; Lou, N. *Chem. Phys. Lett.* **1997**, *265*, 392.

(16) Engelke, F.; Meiwes-Broer, K. H. Laser studies of reaction dynamics. In *Selectivity in Chemical Reactions*; Whitehead, J. C., Ed.; NATO ASI Series 245; Kluwer: Dordrecht, 1988; pp 135−146. Engelke, F.; Meiwes-Broer, K. H. *Chem. Phys. Lett.* **1984**, *108*, 132.

(17) Keller, A.; Lawruszczuk, R.; Soep, B.; Visticot, J. P. *J. Chem. Phys.* **1996**, *105*, 4556.

(18) Han, K.; He, G.; Lou, N. *Chem. Phys. Lett.* **1991**, *178*, 528.

(19) Teule, J. M. Ph.D. Thesis, Vrije Universiteit, Amsterdam, 1997. Teule, J. M.; et al., to be published.

(20) Radzig, A. A.; Smirnov, B. M. *Reference data on atoms, molecules and ions*; Springer-Verlag: Berlin, 1980.

(21) Keijzer, F.; Teule, J. M.; Bulthuis, J.; de Graaff, G. J.; Hilgeman, M. H.; Janssen, M. H. M.; van Kleef, E. H.; van Leuken, J. J.; Stolte, S. *Chem. Phys.* **1996**, *207*, 261; Erratum: **1996**, *210*, 514.

(22) Keijzer, F. Ph.D. Thesis, Katholieke Universiteit, Nijmegen, 1992.

(23) Husain, D.; Roberts, G. *Chem. Phys.* **1988**, *127*, 203.

(24) Keijzer, F.; Bulthuis, J.; de Winter, L. C.; van Kleef, E. H.; Stolte, S. *J. Mol. Spectrosc.* **1995**, *169*, 511.

(25) Altkorn, R.; Zare, R. N. *Annu. Rev. Phys. Chem.* **1984**, *35*, 265.

(26) Steimle, T. C.; Domaille, P. J.; Harris, D. O. *J. Mol. Spectrosc.* **1977**, *68*, 134.

(27) Ernst, W. E.; Schröder, J. O. *Chem. Phys.* **1983**, *78*, 363.

(28) Steimle, T. C.; Domaille, P. J.; Harris, D. O. *J. Mol. Spectrosc.* **1978**, *73*, 441.

(29) Steimle, T. C.; Fletcher, D. A.; Scurlock, C. T. *J. Mol. Spectrosc.* **1993**, *158*, 487.

(30) Stienkemeier, F. Ph.D. Thesis, University of Bielefeld, 1993.

(31) Kinner, W. Ph.D. Thesis, University of Bielefeld, 1990.

(32) *Handbook of Chemistry and Physics*, 77th ed.; CRC Press: Boca Raton, FL, 1996.

(33) Huber, K. P.; Herzberg, G. *Molecular spectra and molecular structure, IV. Constants of diatomic molecules*; Van Nostrand: New York, 1979.

(34) Siegel, A.; Schultz, A. *J. Chem. Phys.* **1980**, *72*, 6227.

(35) Paniagua, M.; Sanz, J. C.; Alvarino, J. M.; Lagana, A. *Chem. Phys. Lett.* **1986**, *126*, 330.

(36) Tsekouras, A. A.; Leach, C. A.; Kalogerakis, K. S.; Zare, R. N. *J. Chem. Phys.* **1992**, *97*, 7220.

(37) Noda, C.; Zare, R. N. *J. Chem. Phys.* **1987**, *86*, 3968.

(38) Meiwes-Broer, K. H. Ph.D. Thesis, University of Bielefeld, 1983.

(39) Griffing, K. M.; Kenney, J.; Simons, J.; Jordan, K. D. *J. Chem. Phys.* **1975**, *63*, 4073.

(40) Hijazi, N. H.; Polanyi, J. C. *J. Chem. Phys.* **1975**, *63*, 2249.

(41) Hartree, W. S.; Simons, J. P.; Gonzalez-Ureña, A. *J. Chem. Soc., Faraday Trans.* **1990**, *86*, 17.

(42) Wüstenbecker, B. Ph.D. Thesis, University of Bielefeld, 1996.

(43) Polanyi, J. C. *J. Chem. Soc., Faraday Discuss.* **1998**, *108*, in press.